Influence of Reduction-Carburization Parameters on the Performance of Supported Molybdenum Carbide Catalysts in Succinic Acid Hydrogenation

M. Abou Hamdan, A. Lilic, M. Vecino-Mantilla, C. Nikitine, L. Vilcocq, M. Jahjah, C. Pinel, N. Perret

Influence of reduction carburization parameters on the performance of supported molybdenum carbide catalysts in succinic acid hydrogenation

Marwa Abou Hamdan [a], Aleksandra Lilic [a], Margarita Vecino-Mantilla [b], Clémence Nikitine [b], Léa Vilcocq [b], Mohamad Jahjah [c], Catherine Pinel [a], Noémie Perret [a,]*

[a] Univ Lyon, Université Claude Bernard Lyon 1, CNRS, IRCELYON, F-69626 Villeurbanne, France

[b] Univ Lyon, Université Claude Bernard Lyon 1, CPE-Lyon, LGPC, F-69616 Villeurbanne, France

[c] LCIO, Laboratoire de Chimie de Coordination Inorganique et Organométallique, Université Libanaise- Faculté des Sciences I, Beyrouth, Liban

ABSTRACT. Molybdenum carbides supported on TiO_2 or ZrO_2 were prepared by temperature programmed reduction carburization method using mixtures of hydrogen and hydrocarbon (methane or ethane). All the materials exhibited molybdenum carbide with cubic crystallographic structure. The carbon content and MoC lattice parameter increased with the increase of hydrocarbon percentage (5-40%) and temperature (600-800°C) during carburization. All catalysts were significantly active in the hydrogenation of succinic acid to butyric acid and γ-butyrolactone. For the first time, a correlation between the degree of carburization and the catalytic activity for

succinic acid hydrogenation was established. The selectivity depends strongly on the support. MoC/TiO_2 favored the formation of butyric acid while MoC/ZrO_2 and bulk MoC generated primarily γ-butyrolactone. The stability of MoC/TiO_2 up to 50 h on stream in continuous reactor was demonstrated, showing the interest of carbide catalysts for future biorefinery processes.

1. INTRODUCTION

Since the report of similarities between the catalytic behavior of platinum noble metals and tungsten metal carbides in 1973,[1] this class of materials, especially group 6 transition metal carbides (TMCs), has gained considerable interest as a promising alternative to noble metals for catalytic applications.[2,3] Their performance is reported in water-gas shift, Fischer-Tropsch, and hydroprocessing reactions such as hydrodesulfurization (HDS) and hydrodenitrogenation (HDN) reactions.[4–6] TMCs have been commonly used as bulk or supported catalysts in gas phase reactions; there are also more recent reports in some liquid phase catalytic applications. Indeed, supported molybdenum carbides have been studied for the transformation of vegetable oils (such as soybean, olive and sunflower oil) in the framework of valorizing sustainable resources.[7–12] The activity of molybdenum carbides was also proven in the transformation of model molecules issued from lignin such as hydrodeoxygenation (HDO) of guaiacol in organic solvent using molybdenum carbide supported on carbon nanofibers (CNF),[13,14] carbon nanotubes (CNT)[15] or AC[16,17] and HDO of phenol over MoC_x supported on hollow carbon spheres.[18] Moreover, Teixeira da Silva and coworkers reported the hydrogenation of levulinic acid derived from cellulose to γ-valerolactone in aqueous solution over Mo_2C supported on CNT.[19] Recently we also reported the high activity of molybdenum carbide supported on TiO_2 in the hydrogenation of succinic acid (SA) which can

be obtained via fermentation of lignocellulosic biomass.[20] Significant amount of butyric acid was formed during the reaction, along with γ-butyrolactone.

Different methods of preparation can be employed for the synthesis of supported molybdenum carbides. Carbon materials, such as AC,[8,15–17,21,22] CNF,[13–15,23,24] and CNT,[15,25] are the most widely used supports. They serve also as carbon source, hence after impregnation, the material usually undergoes a carbon thermal treatment under H_2 or, to a lesser extent, under inert gas. The effect of Mo loading,[24,25] carburization temperature[13,21] and heating rate[13,25] have been studied for this method. When supported on oxides, either an organic carbon or gas precursor must be used. For the first one, a carbon source (e.g. urea, glucose) and a molybdenum precursor are impregnated on the support. This is followed by thermal decomposition under H_2, as reported over Al_2O_3,[26] SBA-15[27] and ZrO_2.[28] The second method is the temperature programmed reduction carburization (TPRC). After impregnation with a molybdenum precursor, the material is placed under a flowing mixture of hydrocarbon/H_2. Mo_2C supported on Al_2O_3,[10,29–32] ZrO_2,[33] and TiO_2[34] have been synthesized using a flow of ca. 20% of CH_4 in H_2. This latter method has been largely studied for the synthesis of bulk catalysts where the synthesis parameters, such as the composition of the gas mixture, the carbon source, heating rate and maximum carburization temperature, play a crucial role on the final properties of the molybdenum carbides.[35–39] However there is no report on the effect of these parameters on the synthesis of supported molybdenum carbide on oxide. It is likely that the support will affect the synthesis due to the support-precursor interaction along with the decrease of the reduction temperature of molybdenum oxide when supported.[40] Therefore studying the influence of the preparation parameters is crucial.

The hydrogenation of succinic acid (SA) has mainly been studied over noble and precious metal supported catalysts. Au[41] and Pd[42] based catalysts usually favor the formation of γ-butyrolactone,

while Re[43,44] favors the formation of tetrahydrofuran. The addition of an oxophilic promoter facilitates ring opening, and high yield of butanediol (up to 83%) can be obtained over ReO_x-Pd/TiO_2.[45] The nature of the precursor, the method of preparation and activation was shown to affect the particle size distribution and metal/support interaction, hence the activity.[42,46] The use of non-noble metal catalysts for this reaction has been scarcely reported.

In the current work, we report the evaluation of some TPRC parameters and their influence on the physicochemical properties of supported molybdenum carbide catalyst and its corresponding catalytic performance in the aqueous phase hydrogenation of SA at 240 °C and 150 bar of H_2. We focused our study on the nature of hydrocarbon used in the reactive gas mixture (CH_4 or C_2H_6), the concentration of the carburizing gas (i.e. % v/v hydrocarbon/H_2) and the maximum carburization temperature in addition to the effect of the nature of the support. We then investigated the stability of the catalysts in a trickle bed reactor.

2. EXPERIMENTAL SECTION

2.1. Catalyst preparation.

The supports used were commercial powders of P25 TiO_2 (specific surface area 55 $m^2\ g^{-1}$, 75% anatase / 25% rutile phases, supplied by Degussa-Evonik), DT51 TiO_2 (specific surface area 92 $m^2\ g^{-1}$, 100% anatase phase, supplied by Tronox) and ZrO_2 (specific surface area 129 $m^2\ g^{-1}$, 90% monoclinic / 10% tetragonal phases, supplied by MEL Chemicals). Extrudates of TiO_2 (specific surface area 55 $m^2\ g^{-1}$, 75% anatase / 25% rutile phases, supplied by Evonik) were also used after being sieved to 200-425 µm (ExTiO_2). The supported molybdenum carbide catalysts were prepared by impregnation followed by TPRC. 1 g of ammonium molybdate tetrahydrate $(NH_4)_6Mo_7O_{24}.4H_2O$ (Aldrich Chemical Co, 99.98% trace metals basis) was used as Mo precursor

and mixed with 5 g of support (10% w/w of Mo/support) in 60 mL of water and stirred for 2 h at room temperature. Water was evaporated in rotavap and the solid was dried in an oven at 80 °C under N_2 flow overnight. For the second step, the powder was introduced into a quartz cell and treated under a reductive-carburizing gas stream (5-40% v/v HC/H_2 with HC: CH_4 or C_2H_6, 60 mL min^{-1}, GHSV = 1090 h^{-1}). The temperature was raised at 0.5 °C min^{-1} until reaching the maximum desired temperature: 600 – 800 °C, held for 2 h, and then cooled down to room temperature under argon. Finally, the catalysts were passivated for 4 h under 1% v/v O_2/N_2 mixture, and then kept in a vial in Ar atmosphere.

2.2. Characterization

The molybdenum loadings of the catalysts were determined by ICP-OES using an ACTIVA instrument (HORIBA JobinYvon). Before analysis, the samples were mineralized by fusion with lithium tetraborate in Pt-Au crucibles at 1100 °C, and then soaked with 20% HCl. The values are reported with an absolute precision of 0.3%.

A LECO micro-analyzer SC144 was used for carbon elemental analyses. After total combustion of the samples at 1050 °C under a flow of helium/oxygen under pressure, the carbon dioxide was quantified by a thermal conductivity detector. The values are reported with an absolute precision of 0.1%.

A Bruker D8A25 X-ray diffractometer equipped with a CuK_α radiation source (λ = 1.54184 Å) was employed to record XRD patterns in the range 2θ = 20-80° at 0.04° s^{-1}. Rietveld refinement was performed using Topas 5 software in order to estimate the lattice parameters (± 0.005 Å) and mean crystallite sizes (d = 4/3 * LVol-IB; ± 1 nm; with LVol-IB the volume averaged column height).

TEM and STEM images were obtained with a TITAN ETEM instrument operated at 80-300 kV, equipped with a X-MAX SDD EDX detector from Oxford-Instrument and a Tridiem ERs GIF from Gatan. Samples were deposited on carbon-coated grids.

The surface chemical composition and oxidation states of Mo in catalyst samples were analyzed by XPS with monochromatized AlK_α source (hν = 1486.6 eV) using a AXIS Ultra DLD KRATOS instrument. The binding energies (± 0.5 eV) were referred to the C1s line set at BE = 284.6 eV. Peaks decompositions, fittings and quantitative determinations were performed using the Casa XPS and Igor Pro software.

BET surface areas of the samples were determined from the N_2 physisorption after desorption at 150 °C for 3 h under ultra-high vacuum (10^{-4} mbar) with ASAP 2020 Micromeritics apparatus. The values are reported with an absolute precision of ± 5 m^2 g^{-1}.

Raman spectra were recorded using a LabRam HR (JobinYvon–Horiba) spectrometer equipped with a CCD detector cooled at -76 °C. Measurements were carried out at room temperature under microscope with a 50 x objective. A Ar^+ laser was used with an exciting line at 514.53 nm. It was previously checked that the samples laser heating was negligible with a power of 100 micro W. A 300 grooves/mm grating was used to disperse light leading to band position accuracy within 4 cm^{-1}.

2.3. Catalytic runs

2.3.1. Reaction in batch reactor

SA with purity above 99% was purchased from Aldrich. The aqueous catalytic hydrogenation experiments were performed using a 300 mL high-pressure batch (Parr 4560) Hastelloy autoclave, equipped with a magnetically driven impeller and a liquid sampling system. The reaction

temperature is monitored by a thermocouple probe which sites inside a thermowell, in the reactor. A 100 mL aqueous solution of SA (0.12-0.14 M; pH = 2.3) and 0.6 g of the catalyst were loaded into the reactor. After sealing, the autoclave was purged three times with Ar, heated up to 240 °C, then pressurized with H_2 up to 150 bar and stirred at 900 rpm. The reactions were conducted for 48 h and samples were collected periodically every 2 h during the day in order to follow the evolution of the reaction.

2.3.2. Reaction in a trickle-bed reactor

SA hydrogenation was performed in a fixed-bed reactor. The stainless steel tube reactor (1.5 mL; ¼ inch × 8 cm) was filled with 1 g of catalyst. It was placed in an oven and purged with N_2. The catalyst was reduced in situ at 300 °C under H_2 flow. Then the reactor was co-fed with a succinic acid aqueous solution using a Shimadzu HPLC pump (0.12 M, 0.05 mL min^{-1}) and H_2 using a Brooks mass flowmeter (25 mL min^{-1}), pressurized at 80 bar with a membrane backpressure regulator, and heated at 260 °C. After the reactor, liquid and gaseous effluents were separated in a collector and liquid samples were taken regularly.

2.3.3. Analytical analysis

Analyses of the reaction products in the liquid samples were performed using a GC Agilent Technologies 6890N with a flame ionization detector employing either a VF-WAXms (30 m × 0.25 mm × 0.25 µm) or an Agilent DB-FFAP (15 m × 0.1 mm x 0.1 µm) columns. The temperature was increased up 190 °C, under helium as a carrier gas.

The concentration of SA was monitored using a Shimadzu LC 20A HPLC connected to UV and RI detectors. The separation was achieved using ICSepCoregel107H column (7.8 × 300 mm)

heated at 40 °C. A solution of H_2SO_4 (0.001 mol L^{-1}) in ultra-pure demineralized water was used as the mobile phase at a flow rate of 0.5 mL min^{-1}.

For SA and the reaction products (butyric acid, γ-butyrolactone, 1,4-butanediol, butanol, tetrahydrofuran), the response factors were determined experimentally with commercial compounds; five solutions with different concentrations, between 0.02 M and 0.13 M, were used for calibration.

SA conversion (%) is based on initial concentration of SA ($[SA]_0$) and defined by:

$$SA\ conversion\ (\%) = \frac{[SA]_0 - [SA]_t}{[SA]_0} \times 100 \quad (1)$$

where $[SA]_t$ refers to the concentration of SA at time *t*.

Selectivity and yield of a product *i* are given by:

$$Selectivity\ (\%) = \frac{[P_i]_t}{[SA]_0 - [SA]_t} \times 100 \text{ and } Product\ yield\ (\%) = \frac{[P_i]_t}{[SA]_0} \times 100 \quad (2)$$

where $[P_i]_t$ refers to the concentration of the product *i* at time *t*.

The carbon balance (CB) is given by:

$$CB\ (\%) = \frac{4*[SA]_t + \sum_i n_i*[P_i]_t}{4*[SA]_0} \times 100 \quad (3)$$

where n_i refers to the number of carbon atoms of the product *i*.

The initial reaction rate was calculated based on the slope of the linear curve, at low conversion (< 40%),

$$V_0(\mathrm{mmol_{Substrate}\ g_{Mo}^{-1}\ h^{-1}}) = \frac{\text{mmole of reactant}}{\text{mass of Mo} \times \text{time}} \quad (4)$$

Repeated reactions delivered conversion and products yield reproducible within ± 3%. Therefore the selectivity is given with an error of ± 3%.

3. RESULTS AND DISCUSSION

3.1. Synthesis and characterization

The catalysts were prepared in two steps. The first one was the impregnation where ammonium heptamolybdate was impregnated on the support. The second step was the TPRC where reduction and carburization occurred at the same time. In order to study the effects of several preparation parameters on the characteristics of the prepared material and its catalytic performance, one parameter was modified at a time, while fixing the others.

Table 1. Surface areas (S_{BET}), Mo and C content (% wt.), anatase/rutile composition (% anatase), mean crystallite size (d) and lattice parameter of cubic fcc MoC of the catalysts.

Entry	Catalyst	S_{BET} (m^2 g^{-1})	% Mo	% C	% anatase	d (nm)	a (Å)
0	$P25TiO_2$	55	-	-	75	-	-
1	$MoC_{10M\text{-}700}/P25TiO_2$	47	9.3	0.8	67	3	4.227
2	$MoC_{20M\text{-}700}/P25TiO_2$	50	9.5	0.6	72	3	4.256
3	$MoC_{40M\text{-}700}/P25TiO_2$	57	9.4	1.2	75	2	4.259
4	$MoC_{5E\text{-}700}/P25TiO_2$	43	9.6	0.8	55	3	4.234
5	$MoC_{10E\text{-}700}/P25TiO_2$	47	9.6	0.8	71	3	4.246
6	$MoC_{20E\text{-}700}/P25TiO_2$	49	9.4	1.2	74	3	4.270
7	$MoC_{20M\text{-}600}/P25TiO_2$	54	9.7	0.3	75	n.a.	n.a.
8	$MoC_{20M\text{-}800}/P25TiO_2$	28	10.0	0.6	n.a.	n.a.	n.a.
9	$MoC_{20E\text{-}600}/P25TiO_2$	54	9.7	0.8	75	3	n.a.
10	$MoC_{20E\text{-}800}/P25TiO_2$	51	8.9	1.4	n.a.	n.a.	n.a.
11	$MoC_{20E\text{-}700}/DT51TiO_2$	84	9.1	1.6	100	2	4.251
12	$MoC_{20E\text{-}700}/ZrO_2$	129	9.2	2.1	-	2	4.187
13	$MoC/ExTiO_2$	47	9.7	4.3	74	3	4.263

n.a.: not available.

The given catalysts notations are denoted as follows: **$MoC_{VN\text{-}T}$/S**, where MoC refers to molybdenum carbide of unspecified stoichiometry for the sake of clarity, V indicates the volumetric percentage of hydrocarbon in hydrogen, N is the first letter corresponding to the nature of hydrocarbon (E for ethane and M for methane), T is the final carburization temperature that was held for 2 h, and S refers to the type of the support (P25 TiO_2, DT51 TiO_2, ZrO_2, $ExTiO_2$). The molybdenum percentage was determined by ICP analysis for all the catalysts and it was always very close to the original loading (around 10% wt. Mo, Table 1).

3.1.1. Effect of hydrocarbon concentration in the reactive gas mixture

To evaluate the effect of hydrocarbons concentration, six catalysts were prepared using different concentrations of hydrocarbon in hydrogen, with either methane or ethane as carbon source. The maximal temperature of carburization was fixed at 700 °C and TiO_2 P25 was used as support. The three catalysts prepared with 5, 10, and 20% v/v C_2H_6/H_2 (entries 4 to 6) are to be compared with 10, 20, and 40% v/v CH_4/H_2 (entries 1 to 3) which have respective equivalent carbon weight compositions.

As shown in Table 1, the carbon weight percentages determined by carbon elemental analysis were affected by the hydrocarbon percentage and range from 0.6% to 1.2%. The lower values obtained when lower hydrocarbon percentage were used (either methane or ethane) indicate either incomplete carburization or a stoichiometry (x) around 0.5 for MoC_x. Whereas the catalysts synthesized with 40% of methane ($MoC_{40M\text{-}700}/P25TiO_2$) and 20% of ethane ($MoC_{20E\text{-}700}/P25TiO_2$) exhibit the highest carbon contents (1.2%) which correspond to the theoretical carbon percentage for a stoichiometry of 1 for 10% wt. MoC/TiO_2.

Raman analysis was done on all the catalysts in order to assess the presence of graphite. The results are either presented in Figure 1, or in Supporting Information (Figure S1). The bands at

145, 196, 397, 440, 517, 605 and 637 cm^{-1} correspond to the anatase and rutile phases of TiO_2.[47] The two catalysts synthesized with 40% of methane (Figure 1-b) and 20% of ethane (Figure 1-a) present two bands at 1345 and 1597 cm^{-1} which are associated to disorder D and tangential G bands of graphitic carbon.[39,48,49] Therefore, for high percentage of hydrocarbon used during the carburization, some free carbon is present at the surface as graphite, as previously reported for syntheses under 20% C_2H_6/H_2 at 700 °C,[20] 10% C_2H_6/H_2 at 800 °C, and 50% CH_4/H_2 at 700 °C.[39] Moreover, the more intense peaks observed for $MoC_{20E\text{-}700}/P25TiO_2$ suggest that the amount of free carbon is more important than on $MoC_{40M\text{-}700}/P25TiO_2$. The four catalysts with lower percentage of hydrocarbon do no present these peaks. Thus, for the catalysts with low amount of carbon, all the carbon is introduced in the molybdenum carbide structure.

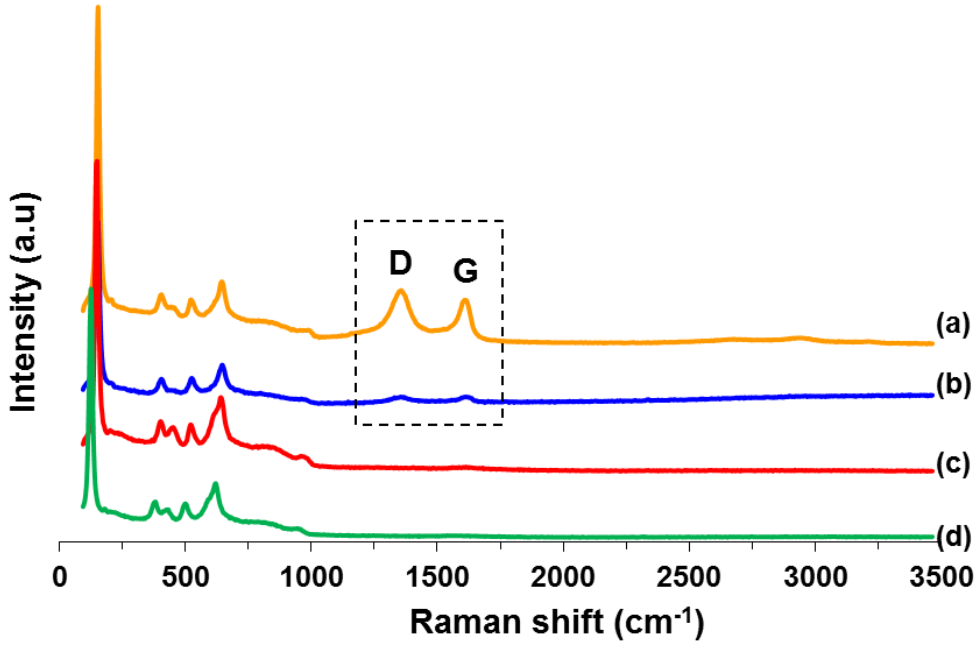

Figure 1. Raman spectra associated with (a) $MoC_{20E\text{-}700}/P25TiO_2$, (b) $MoC_{40M\text{-}700}/P25TiO_2$, (c) $MoC_{5E\text{-}700}/P25TiO_2$ and (d) $MoC_{10M\text{-}700}/P25TiO_2$.

The XRD diffraction patterns corresponding to the catalysts prepared with different methane concentrations are shown in Figure 2, those of the catalysts prepared with ethane are in Supporting Information (Figure S2). The pattern of the bare support P25 TiO_2 is added for comparison. The peaks corresponding to MoC overlapped with the ones of the support, where mainly the peaks corresponding to TiO_2 anatase (PDF 193269) and rutile (PDF 04-006-1919) phases are observed. Rietveld refinement was conducted in order to help with the identification of the different crystalline phases. For the six catalysts, the predominant MoC phase is the face centered cubic structure, with broad peaks at $2\theta = 36.4°$, 42.2° and 61.3° that can be associated with the planes (111), (002) and (022), respectively. The hexagonal $MoC_{0.5}$ was never observed. The crystallite size of MoC was estimated from XRD around 2-3 nm (Table 1).

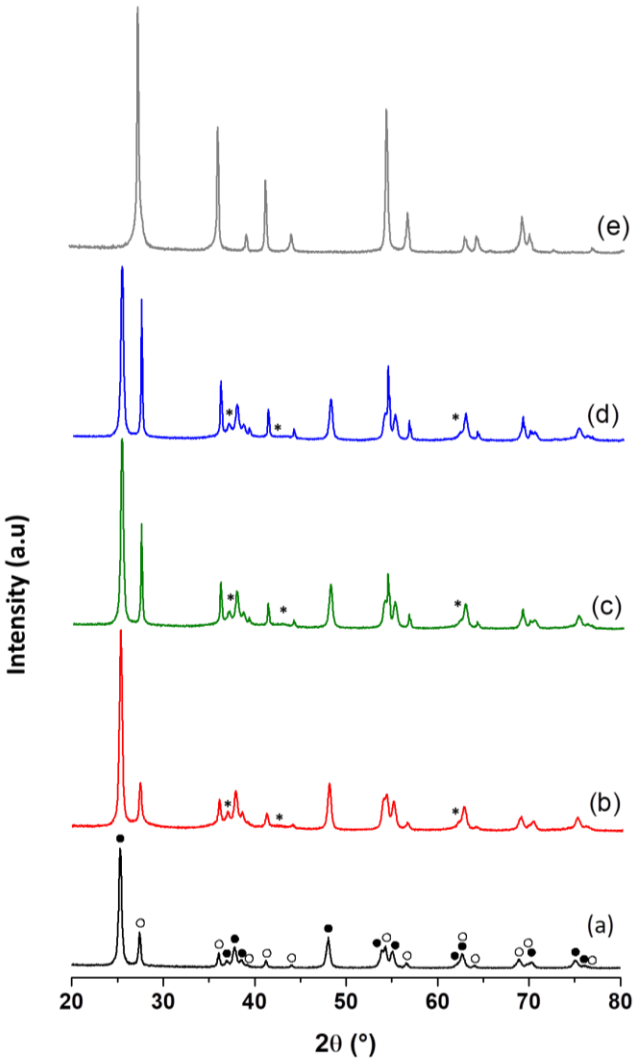

Figure 2. XRD diffraction patterns of (a) P25 TiO_2, b) $MoC_{40M\text{-}700}/P25TiO_2$, c) $MoC_{20M\text{-}700}/P25TiO_2$, d) $MoC_{10M\text{-}700}/P25TiO_2$, and (e) P25 TiO_2 after carburization at 700 °C. Peaks associated with (●) Anatase, (○) Rutile, (*) fcc MoC phase.

The literature on supported molybdenum carbides obtained by carburization with 20% v/v CH_4/H_2 shows the production of either hexagonal (on TiO_2[50], Al_2O_3[32] and carbon nanotubes[19]) or cubic molybdenum carbide (on CNF[24]). We report here the sole formation of cubic molybdenum carbide on TiO_2 when using methane as hydrocarbon. An unsupported catalyst (MoC) was prepared for comparison. It was synthesized via the same preparation procedure of TPRC as $MoC_{20E\text{-}700}/P25TiO_2$, starting with ammonium molybdate tetrahydrate precursor. This resulted in a mixture of hexagonal and cubic MoC (Figure S3). In a like manner, Christopheletti et al. obtained hexagonal molybdenum carbide with 20% v/v CH_4/H_2 at 10 °C min^{-1} till 700 °C, whereas the same procedure for alumina-supported material gave cubic molybdenum carbide.[32] Thus, the presence of the support affect the carburization process and the method of synthesis cannot be directly transferred from bulk to supported catalysts.

Cubic MoC has been shown to be formed via the intermediate MoO_xH_y.[51,52] The oxyhydride exhibits fcc structure with a = 4.10 Å, and after the incorporation of carbon, the lattice parameter increases. The lattice parameters determined for the catalysts (Table 1, Figure 3) are within the range reported for MoC_x with Fm-3m structure (from 4.155 Å for $MoC_{0.5}$ to 4.281 Å for MoC). Moreover, they increase with increasing carbon content, indicating that the ratio C/Mo is also increasing and become close to one for $MoC_{20E\text{-}700}/P25TiO_2$ and $MoC_{40M\text{-}700}/P25TiO_2$. The lattice parameters were slightly higher when using ethane (5% and 20%) instead of methane (10% and 40%), which suggests that the carburization is more efficient. This is in agreement with literature as it is reported that increasing the chain length of the hydrocarbon allows the transformation from oxide to carbide to occur at lower temperature.[36,37] Moreover carbon content has been shown to be higher when using 20% C_2H_6/H_2 than 20% CH_4/H_2 during the synthesis of bulk molybdenum carbide as ethane is easier to decompose than methane.[39]

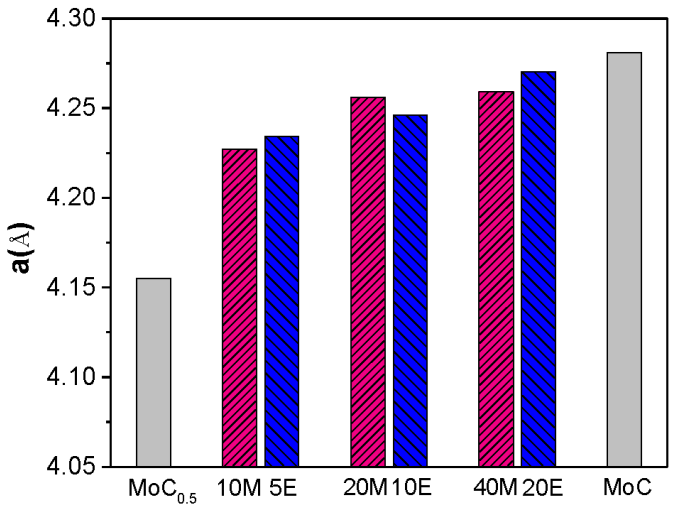

Figure 3. Lattice parameters of cubic MoC associated with $MoC_{10M\text{-}700}/P25TiO_2$ (10M), $MoC_{5E\text{-}700}/P25TiO_2$ (5E), $MoC_{20M\text{-}700}/P25TiO_2$ (20M), $MoC_{10E\text{-}700}/P25TiO_2$ (10E), $MoC_{40M\text{-}700}/P25TiO_2$ (40M), $MoC_{20E\text{-}700}/P25TiO_2$ (20E). Note: the values associated with $MoC_{0.5}$ and MoC correspond to the ones reported in PDF 00-015-0457 and PDF 03-065-8092.

Interestingly, the compositions of anatase and rutile phases are not the same in the different catalysts; they are reported as % anatase (± 3%) in Table 1. Originally, P25 TiO_2 support possesses 75/25 anatase/rutile ratio (Figure 2-a). Carburizing P25 TiO_2 support using 20% v/v C_2H_6/H_2 at 700 °C lead to complete transformation of the anatase phase to rutile, ending up with 100% rutile phase as shown in Figure 2-e. This was expected as anatase phase transforms to rutile at temperature above 500 °C.[53] However in the presence of molybdenum, the anatase phase can be stabilized.[54,55] This is the case for the six catalysts which exhibit at least 55% of anatase. However, in the catalysts prepared with lower hydrocarbon percentages the ratio of anatase to rutile has changed. Therefore the presence of free carbon on the surface also stabilizes the anatase phase where the catalysts with high carbon content conserved the original percentage of anatase, and the catalysts with low carbon content underwent the most significant phase changes. Finally, the crystallite sizes of the anatase phase (27-29 nm) are the same as for the bare support while the ones associated with rutile vary from 11 to 71 nm (Table S1). The BET surface areas determined by N_2

physisorption are reported in Table 1. The values in the range 43-57 m^2 g^{-1} are slightly lower than the support (55 m^2 g^{-1}) which might be due to the treatment at high temperature (700 °C, during carburization) and the incorporation of Mo. Moreover, the decrease in surface area can be linked to the decrease of the percentage of anatase.

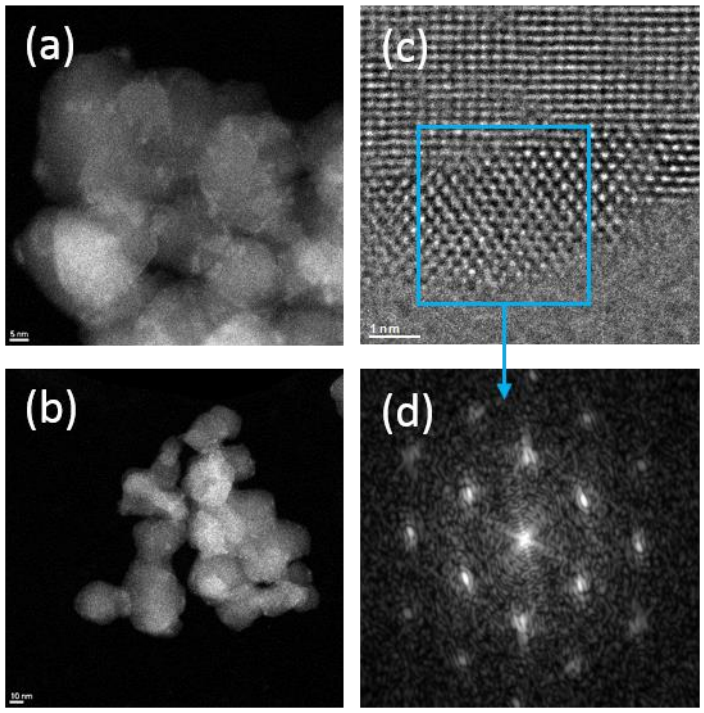

Figure 4. Representative STEM images (a,b), TEM images (c) and electron diffraction (d) of $MoC_{20M\text{-}700}/P25TiO_2$.

STEM and TEM analyses were conducted on some samples and representative pictures of $MoC_{20M\text{-}700}/P25TiO_2$ are shown in Figure 4. The images revealed the presence of small molybdenum carbide particles (< 5 nm), as already determined by XRD analysis. The EDX mapping (Figure S5) also showed the presence of small Mo aggregates (< 5 nm) that are well dispersed on the TiO_2 support. Particles size distributions were determined based on STEM pictures for with $MoC_{10M\text{-}700}/P25TiO_2$ (Figure S5a), $MoC_{20M\text{-}700}/P25TiO_2$ (Figure S5b), $MoC_{40M\text{-}700}/P25TiO_2$ (Figure S5c) and $MoC_{10E\text{-}700}/P25TiO_2$ (Figure S5d). The results show that the average

diameter is in the range 2.5-3.3 nm, independently of the synthesis parameters. The structure and crystal system of some particles were determined by comparing the experimental lattice parameters and angles obtained by electron diffraction with the theoretical values associated with different MoC_x systems ($0.5 \leq x \leq 1$). The results show closest match with MoC of cubic crystal system with Fm-3m space group and a = 4.281 Å. It is however worth noting that a number of cards exist for Fm-3m MoC_x ($0.68 \leq x \leq 1$) with similar lattice parameters (4.266 Å $\leq a \leq$ 4.312 Å). So the formation of molybdenum carbide with Fm-3m structure was confirmed, however, it was not possible to conclude on the stoichiometry of MoC_x by TEM analysis.

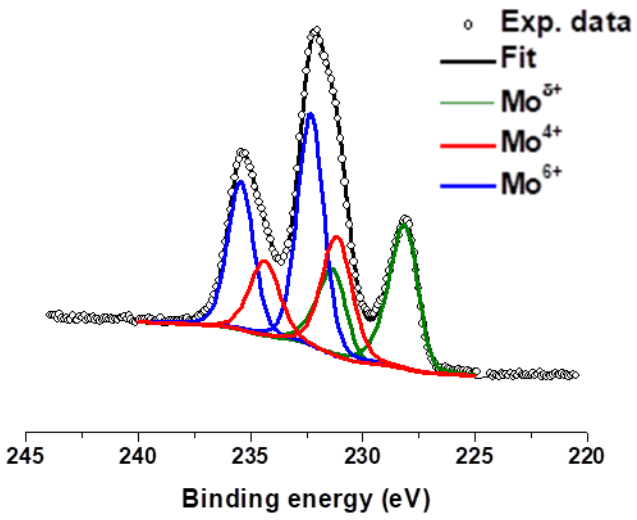

Figure 5. XPS spectrum of Mo 3d of $MoC_{40M\text{-}700}$/P25TiO_2.

In order to gain more information about the Mo and C chemical states in the catalysts and their relative abundance, XPS analysis was done. An example of the Mo 3d spectra for catalyst $MoC_{40M\text{-}}$

$_{700}$/P25TiO$_2$ is presented in Figure 5 and the results obtained for MoC$_{10M-700}$/P25TiO$_2$, MoC$_{40M-700}$/P25TiO$_2$, MoC$_{5E-700}$/P25TiO$_2$ and MoC$_{20E-700}$/P25TiO$_2$ are included in Table 2.

Table 2. XPS analysis: atomic concentration of Mo and abundance of Mo species.

	Atomic concentration %	Mo species %		
Catalyst	Mo	$Mo^{\delta+}$	Mo^{4+}	Mo^{6+}
MoC$_{10M-700}$/P25TiO$_2$	4.7	20	31	49
MoC$_{40M-700}$/P25TiO$_2$	3.9	30	26	44
MoC$_{5E-700}$/P25TiO$_2$	5.2	14	24	62
MoC$_{20E-700}$/P25TiO$_2$	3.0	37	14	49

The Mo 3d spectra of the four catalysts exhibit two peaks at BE = (228.08 eV to 228.26 eV) and (231.07 eV to 231.47 eV) that correspond to Mo 3d$_{5/2}$ and Mo 3d$_{3/2}$ peaks of $Mo^{\delta+}$ ($\delta+ < 1$) which is associated to carbidic Mo in the literature.[56,57] In addition, peaks assigned to Mo^{4+} (BE = 231.1 eV and 234.3 eV) and Mo^{6+} (BE = 232.2 eV and 235.4 eV) were also observed.[58,59] These refer mainly to the passivation layer that is present on the surface of the catalysts.[20] The facts that the catalysts are passivated and that XPS is a surface analysis alter the possibility of quantifying the oxide species that can be associated with incomplete carburization. However, it is possible to compare the catalysts between each other. By comparing the Mo species (Table 2), the catalyst MoC$_{40M-700}$/P25TiO$_2$ and MoC$_{20E-700}$/P25TiO$_2$ possess more $Mo^{\delta+}$ and less molybdenum oxide species (i.e. Mo^{4+} and Mo^{6+}) than the catalyst MoC$_{10M-700}$/P25TiO$_2$ and MoC$_{5E-700}$/P25TiO$_2$. This

is consistent with the XRD results and C content which showed a higher degree of carburization for the former two catalysts. The C 1s spectrum (Figure S6) exhibits a peak at BE = 282.9 eV which confirmed the presence of carbon in the carbidic form.[57] The Mo atomic concentration (Table 2) is lower for $MoC_{40M\text{-}700}/P25TiO_2$ and $MoC_{20E\text{-}700}/P25TiO_2$ which is consistent with the presence of a graphitic layer observed by Raman analysis (Figure 1).

We thus demonstrated that molybdenum carbide particles with a cubic fcc structure were formed on the surface of TiO_2 regardless the nature or percentage of hydrocarbon used. The carbon content, the lattice parameters and the XPS results revealed that the degree of carburization increases with the hydrocarbon percentage, and ethane is a more efficient carburizing agent than methane. Raman analysis also showed the presence of graphite when using high hydrocarbon percent.

3.1.2. Effect of the maximum carburization temperature

To study the effect of the carburization temperature, samples were prepared either at 600 °C or 800 °C with 20% v/v of hydrocarbon/H_2 and they were compared to the samples prepared at 700 °C. As expected, the carbon elemental analyses for the catalysts prepared at different temperatures followed the order: 600 °C ≤ 700 °C ≤ 800 °C with either methane or ethane (Table 1).

When ethane was used as carbon source, Raman analysis (Figure 1 & S1) showed that even at 600 °C some graphite was formed and the amount of graphite increased with the temperature of synthesis, while no graphite was present using 20% v/v CH_4/H_2 for the three temperatures. This is in agreement with Mo et al.[39] who showed by Raman analysis that no carbon deposition was observed when preparing bulk molybdenum carbide at 700 °C using CH_4/H_2 with methane concentration lower than 50%.

It is difficult to observe the cubic molybdenum carbide phase by XRD in case of $MoC_{20M\text{-}600}/P25TiO_2$ (Figure 6-a) and $MoC_{20E\text{-}600}/P25TiO_2$ (Figure S2-d) probably due to the very low amount of this phase or the low crystallinity; hence crystallite size and lattice parameters could not be determined. Rietveld refinement suggests the presence of a small peak at 26.0° referring to MoO_2 phase which emphasizes the incomplete carburization. Therefore, the temperature of 600 °C does not seem efficient to prepare molybdenum carbide with 20% v/v hydrocarbon/H_2. The two catalysts conserved the initial percentage of anatase and surface area, hence the support is stable at 600 °C.

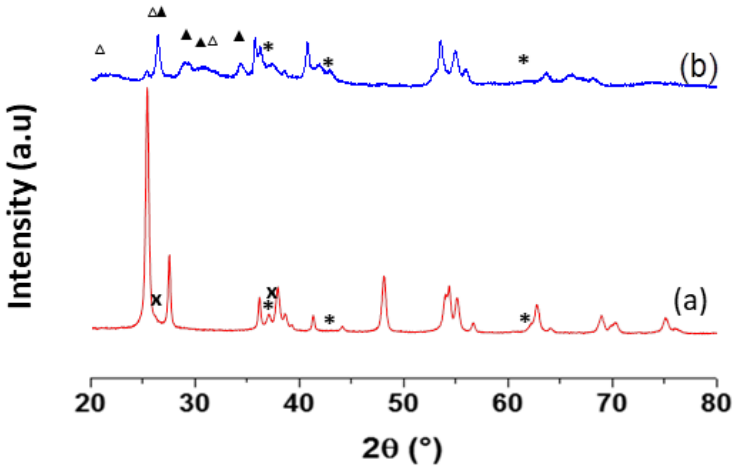

Figure 6. XRD diffraction patterns of a) $MoC_{20M\text{-}600}/P25TiO_2$ and b) $MoC_{20M\text{-}800}/P25TiO_2$. Peaks associated with (▲) Ti_5O_9, (∆) Ti_4O_7, (×) MoO_2, (*) fcc MoC phase.

The catalysts prepared at 800 °C present the peaks associated with cubic MoC in their diffraction patterns (Figure 6-b and Figure S2-e). However, under these conditions, TiO_2 is reduced to Ti_5O_9 and Ti_4O_7. It has been reported that rutile TiO_2 can be reduced and carburized under a CH_4/H_2 gas mixture at high temperature following the sequence: $TiO_2 \rightarrow Ti_5O_9 \rightarrow Ti_4O_7 \rightarrow Ti_3O_5 \rightarrow Ti_2O_3 \rightarrow TiO_xC_y$. The reported TPR profile suggested that at 800 °C, only Ti_5O_9 should be

formed.[60] No peak associated with Ti_3O_5, Ti_2O_3, or TiO_xC_y was observed in the XRD pattern of $MoC_{20M\text{-}800}/P25TiO_2$ and $MoC_{20E\text{-}800}/P25TiO_2$. However, the peaks at 26.4°, 29.0° and 30.7° were attributed to Ti_5O_9. A smaller amount of Ti_4O_7 was also observed at 20.7°, 26.3°, and 31.7°. In the case of ethane hydrocarbon, the transformation of TiO_2 was less prominent than in the case of methane. This could be due to the presence of more carbon that retards the transformation of TiO_2.[60] Due to the difficulty of identification, the lattice parameter and crystallite size of MoC could not be determined for these samples. These changes were accompanied with a decrease in the surface area from 50 $m^2\ g^{-1}$ ($MoC_{20M\text{-}700}/P25TiO_2$) to 28 $m^2\ g^{-1}$ ($MoC_{20M\text{-}800}/P25TiO_2$).

Thus, regardless the carbon source, a treatment at 600 °C is not efficient for the full carburization and at 800 °C the support is altered. As expected, for a given temperature, higher carburization was achieved using ethane instead of methane.

3.1.3. Effect of the nature of the support

Two other supports were used for comparison. DT51 TiO_2 consists of only the anatase phase and has higher surface area (92 $m^2\ g^{-1}$) than P25 TiO_2 (55 $m^2\ g^{-1}$). ZrO_2 is a mixture of monoclinic and tetragonal phases (90%/10%) and has a surface area of 129 $m^2\ g^{-1}$. The catalysts were synthesized using 20% v/v C_2H_6/H_2 at 700 °C.

The analysis of the diffraction pattern associated with the catalyst supported on $DT51TiO_2$ is easier than the ones for the catalysts supported on P25 due to the absence of the peaks corresponding to the rutile phase. The peak corresponding to cubic MoC at $2\theta = 42.2°$ could be clearly observed as shown in Figure S7-c corresponding to $MoC_{20E\text{-}700}/DT51TiO_2$. The lattice parameters obtained match the one associated with MoC (Table 1) but is lower than when using P25 (4.251 Å *vs* 4.270 Å) while the carbon content was higher (1.6% *vs* 1.2%). The STEM and TEM pictures of catalyst $MoC_{20E\text{-}700}/DT51TiO_2$ (Figure 7) show that the catalyst exhibits small

MoC particles dispersed on the surface of the support with an average diameter of 2.5 nm (Figure S5d). As for the catalysts supported on TiO_2 P25, molybdenum carbide exhibits cubic fcc structure, and the particles size was below 5 nm. The carbon content in this catalyst was in excess (1.6%), which is consistent with the graphitic carbon observed by TEM and Raman analysis (Figure S1).

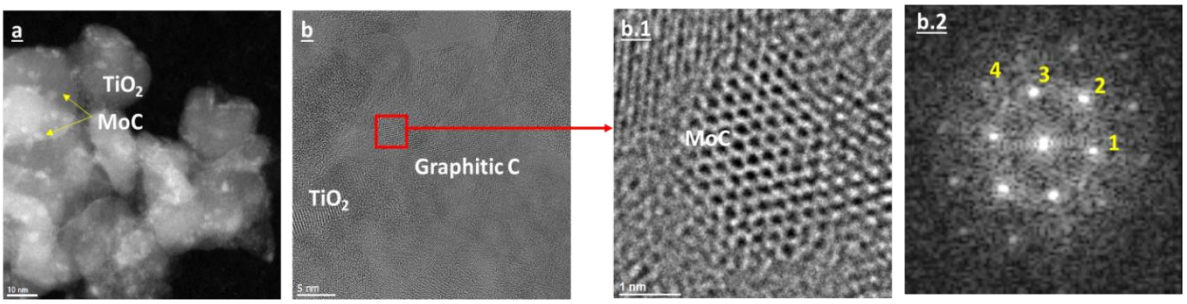

Figure 7. Representative STEM image (a), TEM images (b, b.1), and electron diffraction (b.2) of catalyst $MoC_{20E\text{-}700}/DT51TiO_2$.

For $MoC_{20E\text{-}700}/ZrO_2$, the XRD pattern presents mainly the peaks associated with the ZrO_2 support (Figure S7). The most significant peaks of the monoclinic phase (PDF reference 57157) are at 28.2°, 31.5°, and 49.2°, and those of the tetragonal phase (PDF reference 85322) are at 30.2°, 50.1°, and 60.1°. The Rietveld analysis suggests that molybdenum carbide with a cubic structure is present on the solid. However, the peaks again overlap with the ones from the support. The lattice parameter (a = 4.187 Å, Table 1) is close to the one reported for $MoC_{0.5}$ and lower than all the ones obtained for MoC/TiO_2 (4.227-4.270 Å). This result suggests that the carburization is lower, despite the high carbon content observed by elemental analysis (Table 1). This is in agreement with Adesina et al. who reported that the carburization rate of supported cubic $MoC_{1\text{-}x}$ was the highest on the TiO_2 support followed by SiO_2, ZrO_2, and Al_2O_3,[61] however, the carbon content was not provided. The atomic numbers of Mo (42) and Zr (40) are close to each other,

hence the contrast was too low by microscopy and the STEM-TEM analysis was not conclusive for this sample.

From this part, we conclude that ethane was better than methane as a carburizing gas for the preparation of molybdenum carbides supported on P25 TiO_2 with 20% v/v (with 0.5 °C min^{-1} heating ramp, and GHSV of 1091 h^{-1}). The degree of carburization increased with the temperature and hydrocarbon content, however, at 800 °C the support was drastically altered. Furthermore, the support affects strongly the reduction-carburization and the degree of carburization decreased while the carbon deposition increased following the order P25 TiO_2 < DT51 TiO_2 < ZrO_2.

These different catalysts were evaluated for the hydrogenation of succinic acid in aqueous phase.

3.2. Catalytic hydrogenation of succinic acid

The hydrogenation reactions were carried out at 240 °C and 150 bar, using 600 mg of catalyst and 100 mL of a 0.128 M succinic acid solution (n_{SA}/n_{Mo} = 22). The products were analyzed over two days by GC and HPLC taking periodic liquid samples. We previously showed that MoC supported on TiO_2 can be active for the hydrogenation of succinic acid, where full conversion can be obtained.[20] γ-butyrolactone (GBL) was the major product and was formed simultaneously with a significant amount of butyric acid (BA). Proceeding more in the reaction, GBL was converted mainly to tetrahydrofuran (THF), and BA was converted to butanol (BOL). Few amount of butanediol was obtained at the end of the reaction. GC-MS showed the formation of butane gas in the gas phase accompanied with a decrease in the carbon balance. The reaction pathway is included in Scheme 1.

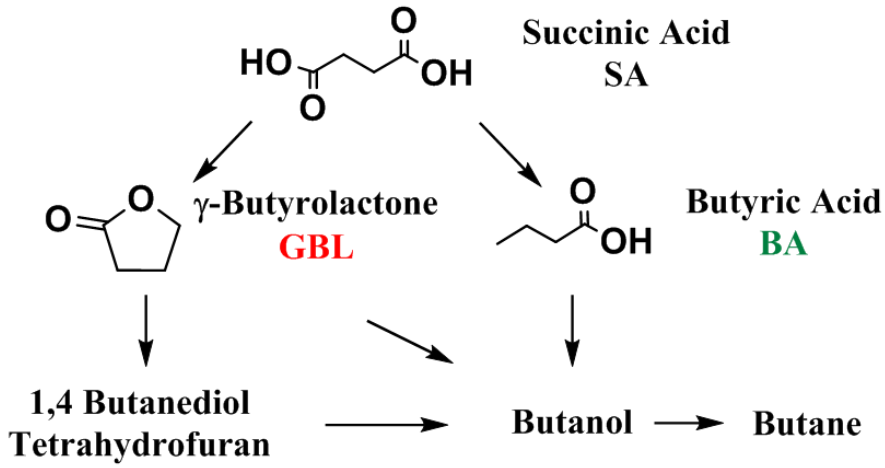

Scheme 1. General reaction scheme for the hydrogenation of succinic acid.

Table 3. Initial rate (V_0) and SA conversion after 46h associated with the catalysts.

Catalyst	V_0 ($mmol_{SA}\ g_{Mo}^{-1}\ h^{-1}$)	SA conversion (%)
$MoC_{10M\text{-}700}/P25TiO_2$	1.7	35
$MoC_{20M\text{-}700}/P25TiO_2$	3.3	70
$MoC_{40M\text{-}700}/P25TiO_2$	4.6	94
$MoC_{5E\text{-}700}/P25TiO_2$	1.8	42
$MoC_{10E\text{-}700}/P25TiO_2$	4.1	81
$MoC_{20E\text{-}700}/P25TiO_2$	4.9	98
$MoC_{20M\text{-}600}/P25TiO_2$	1.7	35
$MoC_{20M\text{-}800}/P25TiO_2$	7.8	99
$MoC_{20E\text{-}600}/P25TiO_2$	1.5	31
$MoC_{20E\text{-}800}/P25TiO_2$	5.2	99
$MoC_{20E\text{-}700}/DT51TiO_2$	8.0	99
$MoC_{20E\text{-}700}/ZrO_2$	2.4	58
MoC[a]	3.1	73

[a]0.06 g of catalyst

3.2.1. Influence of hydrocarbon concentration in the reductive-carburizing gas

To test the influence of hydrocarbon concentration in the reductive-carburizing gas on the catalytic activity, reactions were done using the catalysts prepared at the same temperature but with different methane and ethane concentrations: $MoC_{10M\text{-}700}/P25TiO_2$, $MoC_{20M\text{-}700}/P25TiO_2$, $MoC_{40M\text{-}700}/P25TiO_2$ and $MoC_{5E\text{-}700}/P25TiO_2$, $MoC_{10E\text{-}700}/P25TiO_2$, and $MoC_{20E\text{-}700}/P25TiO_2$.

The succinic acid conversion versus time is reported in Figure 8-a. The initial rates and final conversions are included in Table 3. After 46 h, 35% of SA was converted using $MoC_{10M\text{-}700}/P25TiO_2$, whereas over $MoC_{20M\text{-}700}/P25TiO_2$, 70% of SA was converted, and 94% conversion was observed with $MoC_{40M\text{-}700}/P25TiO_2$. On the other hand, 42% of SA was converted using $MoC_{5E\text{-}700}/P25TiO_2$ after 46 h, and 81% was converted with $MoC_{10E\text{-}700}/P25TiO_2$, whereas almost full conversion was achieved with $MoC_{20E\text{-}700}/P25TiO_2$. The initial rates follow the same order as the conversions: $MoC_{20E\text{-}700}/P25TiO_2 > MoC_{40M\text{-}700}/P25TiO_2 > MoC_{10E\text{-}700}/P25TiO_2 > MoC_{20M\text{-}700}/P25TiO_2 > MoC_{5E\text{-}700}/P25TiO_2 > MoC_{10M\text{-}700}/P25TiO_2$. The catalysts activity increased with the increase of methane or ethane percentage in the gas mixture during their reduction-carburization. This was expected as the catalysts prepared with the higher concentrations were the ones with the more complete carburization as shown by elemental analysis, XRD and XPS, in the previous section. Furthermore, the catalysts synthesized with the same amount of carbon in the feed present slightly higher conversions and initial rates in the case of ethane hydrocarbon compared to methane as revealed in Figure 8-a and Table 3. This is also consistent with the higher degree of carburization observed when using ethane during the synthesis. These results demonstrate a direct link between the degree of carburization and the activity of the catalyst.

Figure 8-b represents the selectivity to the main products obtained over the different catalysts for conversion < 80%. The products distribution is mainly composed of GBL and BA whatever

the catalysts. GBL is the major product (53-68% selectivity) and BA is the second main product (25-36% selectivity), which is contrary to usual literature.[41,42,45,46,62–65] Indeed, small quantity of butyric acid has been reported for the hydrogenation of succinic acid in liquid phase over noble metal catalysts (< 3%).[45,63,64] BA might be formed by successive hydrogenation/dehydration, without desorption of the intermediate aldehyde[20, 66]. Both products are formed simultaneously from the beginning of the reaction and constant selectivity (± 5%) is observed up to 80% conversion. The carbon balance was always ca. 95% regardless the catalyst, indicating that there is no loss of carbon in gas phase. Low amounts of THF, BOL, and traces of BDO were detected at the end of the reactions at higher conversion. It is hard to evaluate the influence of hydrocarbon concentration on the selectivity to GBL and BA since the level of selectivity is close among all catalysts, except lowest GBL selectivity in favor to BA for catalyst $MoC_{20E\text{-}700}/P25TiO_2$ which is the most carburized. There is a slightly more THF and butanol at higher percentage of hydrocarbon.

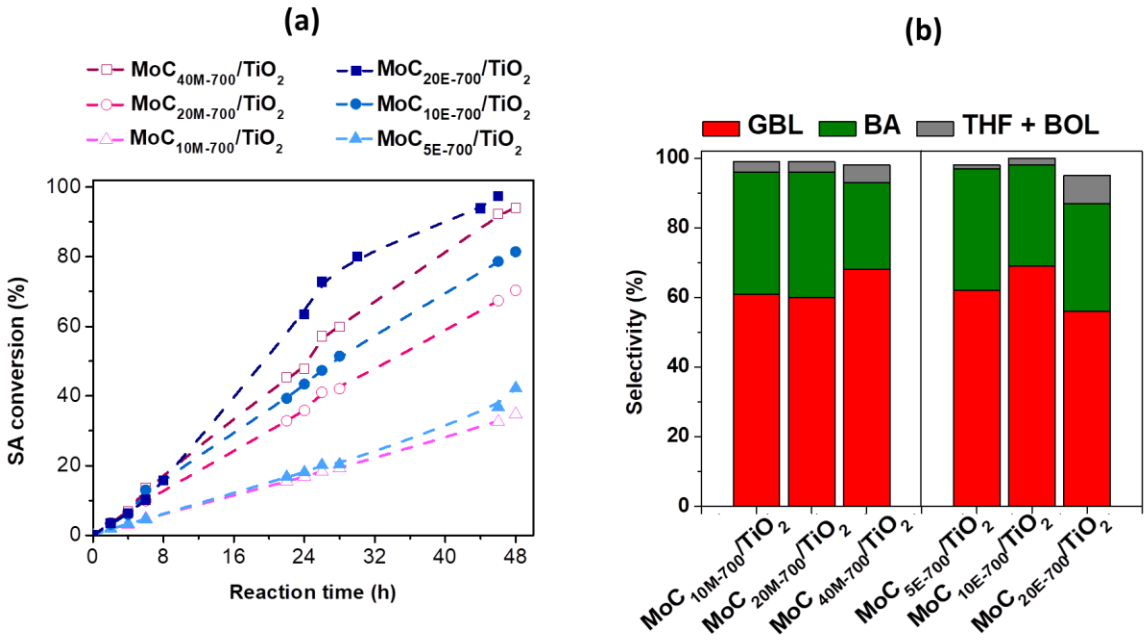

Figure 8. Succinic acid conversion (a) and selectivity (b) to the main products (conversion ≤ 80%), obtained over the catalysts prepared with different hydrocarbons concentrations with $P25TiO_2$.

3.2.2. Influence of carburizing temperature

Regardless the hydrocarbon, the catalysts prepared at 600 °C that were less carburized were much less active in the reaction of hydrogenation of SA (31-35% conversion after 46 h) than the catalysts prepared at 700 or 800 °C as shown in Figure 9-a and Table 3. On the other hand, the catalysts prepared at 800 °C gave full conversion after 46 h. The initial rates (Table 3) follow the order: $MoC_{20M\text{-}800}/P25TiO_2$ > $MoC_{20E\text{-}800}/P25TiO_2$ > $MoC_{20E\text{-}700}/P25TiO_2$ > $MoC_{20M\text{-}700}/P25TiO_2$ > $MoC_{20M\text{-}600}/P25TiO_2$ > $MoC_{20E\text{-}600}/P25TiO_2$. Thus, in all cases the catalysts that are carburized at higher temperature were more active in SA hydrogenation reaction, due to a higher degree of carburization. Moreover the catalysts carburized at higher temperature might also exhibit more oxygen vacancies and higher metal-support interaction.

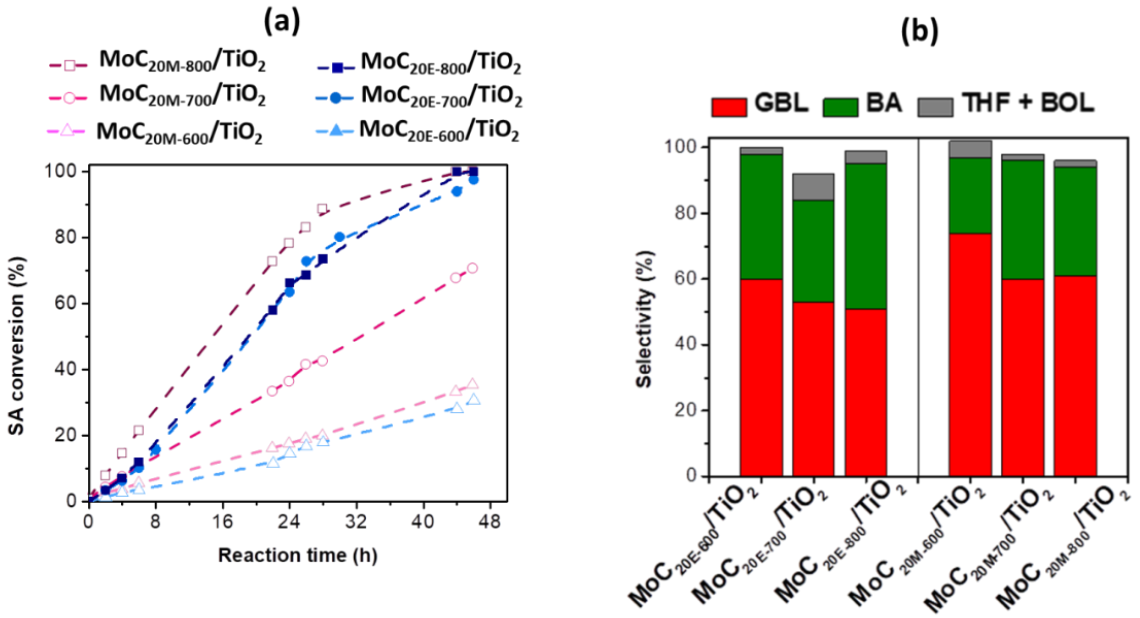

Figure 9. Succinic acid conversion (a) and selectivity (b) to the main products (conversion ≤ 80%) obtained over catalysts prepared at different temperatures with $P25TiO_2$.

With these catalysts, GBL is the main product, with slight differences in the level of selectivity (Figure 9-b). When comparing the selectivity to products obtained by each of the three catalysts prepared with the same hydrocarbon, the selectivity levels were close. Though, by comparing the six catalysts, the highest GBL selectivity is produced with catalyst $MoC_{20M\text{-}600}/P25TiO_2$ (74% selectivity at 46 h), whereas the lowest is 51% at 46 h for $MoC_{20E\text{-}800}/P25TiO_2$.

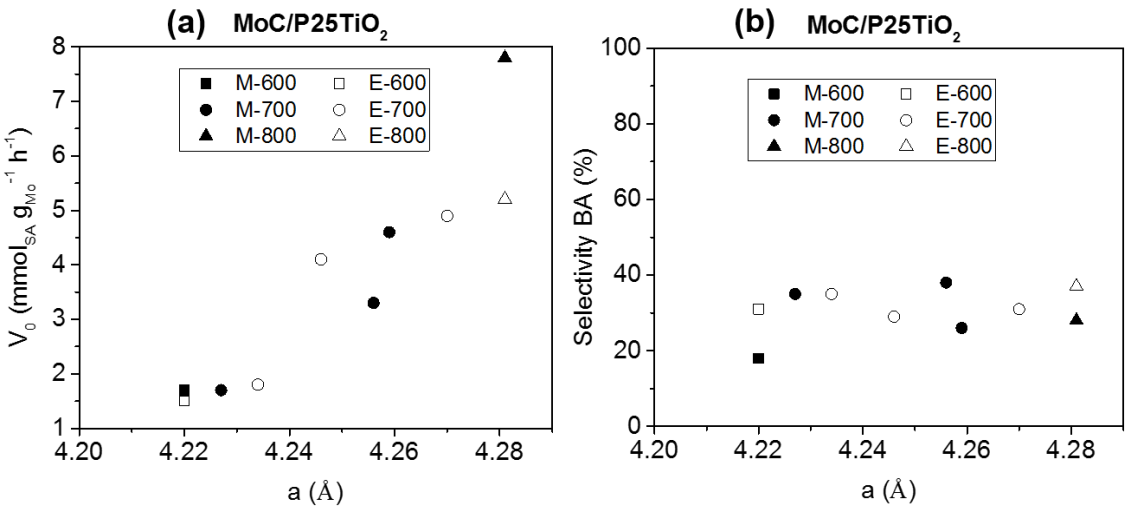

Figure 10. (a) Initial rate (V_0) and (b) selectivity towards BA in function of lattice parameters, for molybdenum carbide supported on $P25TiO_2$. Note: The symbols refer to the catalysts synthesized with methane (M) and ethane (E), at 600 °C, 700 °C and 800 °C, irrespectively of the concentration of hydrocarbon.

Figure 10 combine the results presented in the previous sections. The initial rates associated with the catalysts supported on $P25TiO_2$ are plotted in function of the lattice parameter of MoC (Figure 10-a). The lattice parameters had to be estimated for some of the catalysts (Table S2). The results reveal that the activity of the catalyst increases with the lattice parameter of MoC. The reduction carburization parameters (nature and concentration of hydrocarbon, temperature) affect the degree of carburization and the lattice parameter. Therefore, for the same support, the catalysts which are the most carburized, i.e. which exhibit a stoichiometry close to MoC, are the most active.

$MoC_{20M\text{-}800}/P25TiO_2$ does not fit with this curve, however this can be attributed to the important modification of the support under these synthesis conditions. The presence of Ti_5O_9 in high proportion prevents us to compare it directly with the other catalysts and this result suggests an influence of the support on the activity. It can be seen from Figure 10-b, that the selectivity to BA does not depend on the lattice parameter, i.e. the reduction carburization parameters.

It is difficult to compare the results with the literature, in term of TOF, as there are reported with varied units and reaction conditions were usually different. Nevertheless, the initial rates reported in Table 3 are of the same order of magnitude than Cu-Mg_2SiO_4[67]. However they remain lower by a factor between 10 and 1000, than those reported previously for precious metal supported catalysts (e.g. Pd/C[67], Au/TiO_2[41], Ru-Sn/GAC[68]).

3.2.3. Effect of the support

The effect of the nature of the support on the performance of the catalysts was investigated. For comparison TiO_2 from a different supplier was tested (DT51). ZrO_2 was employed as it is a stable oxide support, already used for levulinic acid hydrogenation with supported noble metal catalysts [69]. Finally, bulk molybdenum carbide catalyst was also evaluated.

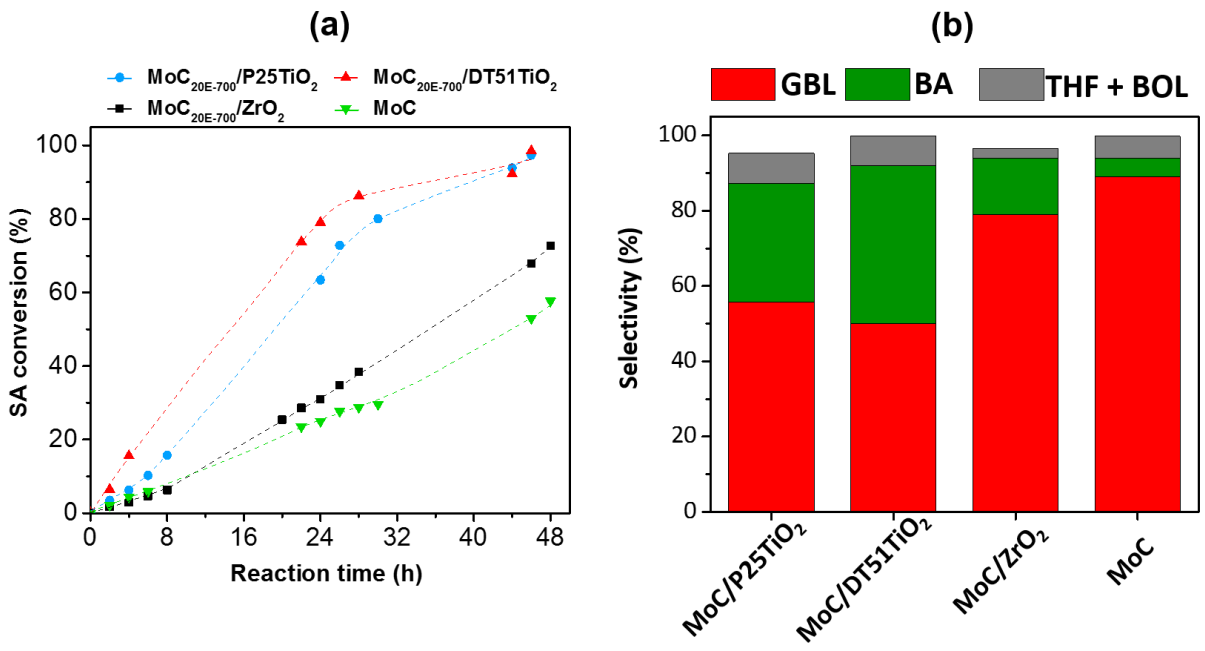

Figure 11. Succinic acid conversion (a) and selectivity (b) to the main products (conversion ≤ 80%) obtained over $MoC_{20E-700}/P25TiO_2$, $MoC_{20E-700}/DT51TiO_2$, $MoC_{20E-700}/ZrO_2$, and MoC.

Figure 11 shows the conversion of SA and selectivity to the products obtained over the four catalysts. Full conversion was achieved over $MoC_{20E-700}/DT51TiO_2$ and $MoC_{20E-700}/P25TiO_2$ at the end of the reactions. MoC/ZrO_2 and MoC were less efficient and SA conversion reached only 58% and 73% respectively. The initial rates (Table 3) follow the order: $MoC_{20E-700}/DT51TiO_2 > MoC_{20E-700}/P25TiO_2 >> MoC \sim MoC/ZrO_2$. When gathering all the results together (Figure S8-a), the activity observed for MoC/ZrO_2 and MoC are in line with the results obtained with $MoC/P25TiO_2$. Indeed, the low activity of MoC/ZrO_2 can be attributed to its low degree of carburization. Moreover MoC presents a similar activity as $MoC/P25TiO_2$ with comparable lattice parameter. However it is also clear, from Figure S8-a, that, for similar degree of carburization, the catalysts are more active when using $DT51TiO_2$ than the other supports, hence the nature of the support plays also a crucial role.

At 80% of conversion, selectivity of 55% to GBL and 31% to BA were obtained when using TiO_2 P25, and 50% to GBL and 42% to BA with TiO_2 DT51. Therefore $MoC_{20E\text{-}700}/DT51TiO_2$ is slightly more selective to BA than $MoC_{20E\text{-}700}/P25TiO_2$ with a ratio BA/GBL of ca. 0.8 and 0.5, respectively. The more important difference in products distribution is with ZrO_2-supported catalyst which shows remarkable selectivity to GBL (80%) with less than 20% of BA (Figure 11-b & Figure S8-b). This behavior is closer to the one obtained with the unsupported MoC catalyst. For this latter one, the selectivity to GBL is even more pronounced and reached 89% while BA selectivity was very low (< 5%). When comparing unsupported Mo_2C with the alumina supported catalyst, Christofoletti et al.[32] showed that Mo_2C/Al_2O_3 was more active than the bulk catalyst in methane steam reforming. They suggested that the greater activity of the supported catalysts may be related to the higher activity of the cubic MoC species present in Mo_2C/Al_2O_3 samples, compared to the hexagonal Mo_2C species present in the unsupported material, or to the higher dispersion of the cubic MoC in the supported catalyst, knowing that the alumina support was not active in the reaction.

The above results show that for SA hydrogenation reaction the support affect the activity and selectivity delivered by molybdenum carbide catalysts. It is difficult to conclude on the exact role of the support, as the degree of carburization, the amount of carbon and the crystallographic phase also impact the catalytic results. However it seems that the activity increases with the degree of carburization, but it can also be improved when using $DT51TiO_2$. The adsorption of H_2 on molybdenum carbide surface usually occurs on metallic like sites (exposed Mo and C) while adsorption of the substrate occurs on vacancy sites.[70] The catalysts with higher degree of carburization exhibit more metallic surface (Mo species with lower degree of oxidation) which favor H_2 uptake and dissociation.[71] The formation of BA requires a strong adsorption of the

intermediate with the surface. The results show that the interaction is stronger on TiO_2-carbide, than on ZrO_2-carbide or bulk molybdenum carbide. The formation of BA occurs in the presence of well carburized particles of cubic MoC dispersed on TiO_2, hence the active sites must be at the interface support-carbide and associated with vacancy (oxygen, carbon) sites.

3.2.4. Reaction in trickle-bed

Butyric acid and γ-butyrolactone have many uses in industries. For example GBL is used as a solvent in chemical industry and as an intermediate in the production of herbicides, rubbers, cosmetics and pharmaceuticals industry.[72] BA is mainly used in the animal feed sector and in chemical industry for the manufacture of cellulose acetate butyrate for plastics. Currently, BA is mainly produced by oxidation of butyraldehyde that is obtained from propylene derived from crude oil by oxosynthesis, with an annual production which should reach 75 kt by 2020.[73] Nevertheless, as for all derivatives of crude oil, concerns arise about the increasing petroleum prices and availability along with the growing need for clean chemical. The production of BA and GBL from renewable resources are receiving growing interest from the scientific community and the industry. In order to develop a catalytic process for the conversion of bio-succinic acid to GBL and BA, the stability of the catalyst was assessed.

Extrudates of TiO_2 were used as support after being crushed and sieved to 200-425 µm. After impregnation, a temperature programmed reduction carburization was conducted with 20% C_2H_6/H_2 up to 700 °C. The main properties of the catalyst $MoC/ExTiO_2$ (Table 1, entry 13) are similar to the ones of $MoC_{20E\text{-}700}/P25TiO_2$, reported in section III.1. They both exhibit a mixture of anatase/rutile (percentage of anatase = 74%) and a surface area around 50 $m^2\ g^{-1}$. It is however worth noting that the carbon content is higher (4.3 % vs. 1-2 %). We have previously shown in III.1.3 that the nature of the support affect the carburization and carbon content. The size of the

extruded might also be playing a crucial role, and this would require further investigation. First the catalyst was tested in batch reactor at 240 °C and under 150 bar of H_2 (Figure S9). The results are comparable to what was obtained with $MoC_{20E\text{-}700}/P25TiO_2$ in term of activity and selectivity to BA (35% vs. 31%). Therefore the carbon content, along with the amount of free carbon on the surface, do not seem to affect the catalytic results. Hence the free carbon does not block the active sites.

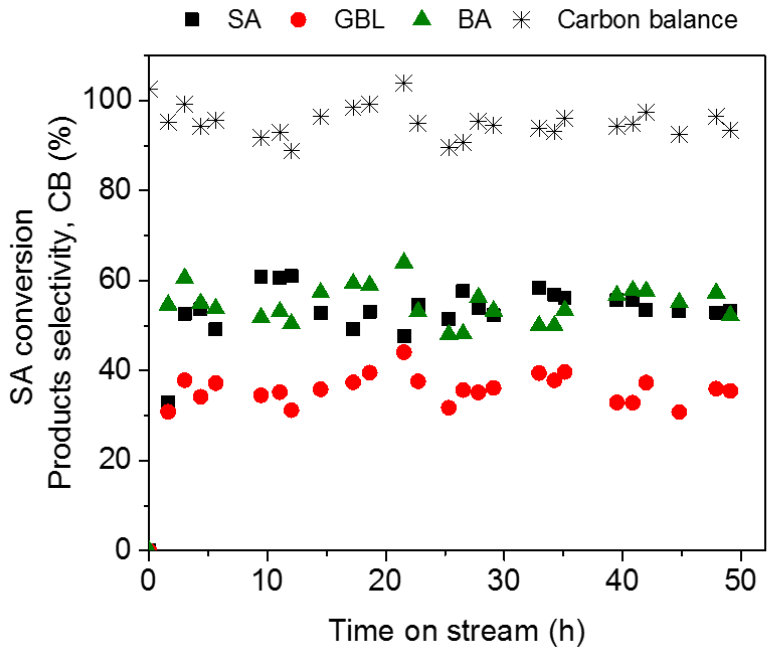

Figure 12. Hydrogenation of succinic acid over $MoC/ExTiO_2$, in a trickle-bed reactor, at 260 °C and under 80 bar H_2: temporal evolution of the conversion of SA, selectivity to BA, selectivity to GBL and carbon balance (CB). Aqueous solution of SA (0.12M, 0.05 mL min^{-1}), 1 g of catalyst.

The stability test was conducted in a trickle-bed reactor in order to examine conversion/selectivity over a long period without air exposure of the catalyst. For technical reasons, it was not possible to carry out the reaction under similar conditions to batch reactor.

Indeed, the reaction was conducted at 260 °C and under 80 bar H_2. The catalytic results obtained over MoC/ExTiO_2 are presented in Figure 12. The conversion reached ca. 55% after 2 h and remained stable up to 50 h. BA and GBL were the two main products observed. BOL and THF were observed as traces, hence there are not included in Figure 12. The yield of BA (30%) and GBL (20%) also remained constant with time. The selectivity to BA (ca. 55%) was higher than the one observed in batch reactor at the same conversion (35%). However, for this continuous test, a reaction rate of 3.9 $mmol_{SA}.g_{Mo}^{-1}.h^{-1}$ can be estimated, which is comparable to what was obtained in batch reactor with MoC/ExTiO_2 (3.4 $mmol_{SA}.g_{Mo}^{-1}.h^{-1}$), while the H_2 pressure is twice as low. Nevertheless it may not be possible to compare the results obtained in batch and in continuous reactors in more details. Indeed, the catalyst pre-treatment and reaction conditions (e.g. H_2 pressure, contact time, transfer resistances) were different. Moreover the design of the reactor might also affect the catalytic results, e.g. the contact times were different.

To conclude, the stability of this catalyst confirms the potential of carbide catalysts for the conversion of bio-based molecules under reductive atmosphere.

4. CONCLUSIONS

For the first time, the effect of the composition of the gas mixture, the carbon source and the maximum carburization temperature on the synthesis of molybdenum carbide supported on oxide were studied. Molybdenum carbides were prepared using either methane or ethane as carbon source, changing the concentration of hydrocarbon in the reactive gas and the carburizing temperature in addition to the support nature. The catalysts were characterized by ICP, XRD, carbon elemental analysis, TEM, STEM, XPS, Raman, and BET. Small crystallites of cubic MoC were obtained, independently of the synthesis conditions. The characterization showed an increase in degree of carburization with hydrocarbon percentage and temperature. Ethane carbon source

was more efficient than methane in preparing well carburized catalyst with Mo/C ratio close to one.

Screening for the best preparation conditions for the use of molybdenum carbide catalysts in SA hydrogenation showed that the catalytic activity increased with the lattice parameter of MoC and degree of carburization. The catalysts prepared at low carburization temperature (600 °C), were much less active than the ones prepared at 700 °C or 800 °C. However, the high temperature led to drastic modifications of the P25 TiO_2 support. The support plays a significant role in the activity and selectivity of the catalyst. The hydrogenation of SA generated mainly γ-butyrolactone and butyric acid. Carbides are promising alternative catalysts to noble-based metal ones. Molybdenum is far less costly than noble metal, for example it is 2700 times less expensive than palladium. Finally the catalyst was stable when used in continuous reactor for 50 h on stream.

AUTHOR INFORMATION

Corresponding Author

*Noémie Perret – Institut de Recherches sur la Catalyse et l'Environnement de Lyon - noemie.perret@ircelyon.univ-lyon1.fr

ABBREVIATIONS

TMC, transition metal carbides; HDS, hydrodesulfurization; HDN, hydrodenitrogenation; AC, activated carbon; CNF, carbon nanofibers; CNT, carbon nanotubes; HDO, hydrodeoxygenation; TPRC, temperature programmed reduction carburization; SA, succinic acid; GBL, γ-Butyrolactone, THF, tetrahydrofuran; BA, butyric acid; BOL, butanol.

ACKNOWLEDGMENT

The authors acknowledge the Service Scientifiques of IRCELYON for their help in the characterization of the catalysts. They also acknowledge Patrick Jame and Erik Bonjour (ISA, Institute of Science Analytical) for the Carbon elemental analyses and Frédéric Bornette (LGPC) for the design of continuous reactor.

Funding Sources

This research did not receive any specific grant from funding agencies in the public, commercial, or not-for-profit sectors.

REFERENCES

(1) Levy, R. B.; Boudart, M. Platinum-like behavior of tungsten carbide in surface catalysis. *Science* **1973**, *181*, 547–549.

(2) Hwu, H. H.; Chen, J. G. Surface chemistry of transition metal carbides. *Chem. Rev.* **2005**, *105* (1), 185–212.

(3) Alexander, A.-M.; Hargreaves, J. S. J. Alternative catalytic materials: Carbides, nitrides, phosphides and amorphous boron alloys. *Chem. Soc. Rev.* **2010**, *39* (11), 4388–4401.

(4) Dolce, G. M.; Savage, P. E.; Thompson, L. T. Hydrotreatment activities of supported molybdenum nitrides and carbides. *Energy Fuels* **1997**, *11* (3), 668–675.

(5) Vo, D.-V. N.; Adesina, A. A. Fischer–Tropsch Synthesis over Alumina-Supported Molybdenum Carbide Catalyst. *Appl. Catal. Gen.* **2011**, *399* (1–2), 221–232.

(6) Patt, J.; Moon, D. J.; Phillips, C.; Thompson, L. Molybdenum carbide catalysts for Water–Gas Shift. *Catal. Lett.* **2000**, *65*, 193–195.

(7) Choi, J.-S.; Zacher, A. H.; Wang, H.; Olarte, M. V.; Armstrong, B. L.; Meyer, H. M.; Soykal, I. I.; Schwartz, V. Molybdenum carbides, active and in situ regenerable catalysts in hydroprocessing of fast pyrolysis bio-oil. *Energy Fuels* **2016**, *30*, 5016–5026.

(8) Han, J.; Duan, J.; Chen, P.; Lou, H.; Zheng, X. Molybdenum carbide-catalyzed conversion of renewable oils into diesel-like hydrocarbons. *Adv. Synth. Catal.* **2011**, *353* (14–15), 2577–2583.

(9) Kim, S. K.; Yoon, D.; Lee, S.-C.; Kim, J. Mo_2C/Graphene nanocomposite as a hydrodeoxygenation catalyst for the production of diesel range hydrocarbons. *ACS Catal.* **2015**, *5* (6), 3292-3303.

(10) Sousa, L. A.; Zotin, J. L.; Teixeira da Silva, V. Hydrotreatment of sunflower oil using supported molybdenum carbide. *Appl. Catal. Gen.* **2012**, *449*, 105–111.

(11) Wang, H.; Yan, S.; Salley, S. O.; Ng, K. Y. S. Hydrocarbon fuels production from hydrocracking of soybean oil using transition metal carbides and nitrides supported on ZSM-5. *Ind. Eng. Chem. Res.* **2012**, *51* (30), 10066–10073.

(12) Qin, Y.; Chen, P.; Duan, J.; Han, J.; Lou, H.; Zheng, X.; Hong, H. Carbon nanofibers supported molybdenum carbide catalysts for hydrodeoxygenation of vegetable oils. *RSC Adv.* **2013**, *3* (38), 17485–17491.

(13) Ochoa, E.; Torres, D.; Moreira, R.; Pinilla, J. L.; Suelves, I. Carbon nanofiber supported Mo_2C catalysts for hydrodeoxygenation of guaiacol: The importance of the carburization process. *Appl. Catal. B Environ.* **2018**, *239*, 463–474.

(14) Jongerius, A. L.; Gosselink, R. W.; Dijkstra, J.; Bitter, J. H.; Bruijnincx, P. C. A.; Weckhuysen, B. M. Carbon nanofiber supported transition-metal carbide catalysts for the hydrodeoxygenation of guaiacol. *ChemCatChem* **2013**, *5* (10), 2964–2972.

(15) Santillan-Jimenez, E.; Perdu, M.; Pace, R.; Morgan, T.; Crocker, M. Activated carbon, carbon nanofiber and carbon nanotube supported molybdenum carbide catalysts for the hydrodeoxygenation of guaiacol. *Catalysts* **2015**, *5* (1), 424–441.

(16) Liu, S.; Wang, H.; Smith, K. J.; Kim, C. S. Hydrodeoxygenation of 2-Methoxyphenol over Ru, Pd, and Mo_2C catalysts supported on carbon. *Energy Fuels* **2017**, *31* (6), 6378–6388.

(17) Ma, R.; Cui, K.; Yang, L.; Ma, X.; Li, Y. Selective catalytic conversion of guaiacol to phenols over a molybdenum carbide catalyst. *Chem. Commun.* **2015**, *51* (51), 10299–10301.

(18) Engelhardt, J.; Lyu, P.; Nachtigall, P.; Schüth, F.; García, Á. M. The influence of water on the performance of molybdenum carbide catalysts in hydrodeoxygenation reactions: A Combined theoretical and experimental study. *ChemCatChem* **2017**, *9* (11), 1985–1991.

(19) Mai, E. F.; Machado, M. A.; Davies, T. E.; Lopez-Sanchez, J. A.; Teixeira da Silva, V. Molybdenum carbide nanoparticles within carbon nanotubes as superior catalysts for γ-valerolactone production via levulinic acid hydrogenation. *Green Chem.* **2014**, *16* (9), 4092–4097.

(20) Abou Hamdan, M.; Loridant, S.; Jahjah, M.; Pinel, C.; Perret, N. TiO_2-supported molybdenum carbide: An active catalyst for the aqueous phasehydrogenation of succinic acid. *Appl. Catal. Gen.* **2019**, *571*, 71–81.

(21) Wang, H.; Liu, S.; Smith, K. J. Synthesis and hydrodeoxygenation activity of carbon supported molybdenum carbide and oxycarbide catalysts. *Energy Fuels* **2016**, *30* (7), 6039–6049.

(22) He, L.; Qin, Y.; Lou, H.; Chen, P. Highly dispersed molybdenum carbide nanoparticles supported on activated carbon as an efficient catalyst for the hydrodeoxygenation of vanillin. *RSC Adv* **2015**, *5* (54), 43141–43147.

(23) Jongerius, A. L.; Bruijnincx, P. C. A.; Weckhuysen, B. M. Liquid-phase reforming and hydrodeoxygenation as a two-step route to aromatics from lignin. *Green Chem.* **2013**, *15* (11), 3049–3056.

(24) Souza Macedo, L.; Oliveira, R. R.; van Haasterecht, T.; Teixeira da Silva, V.; Bitter, H. Influence of synthesis method on molybdenum carbide crystal structure and catalytic performance in stearic acid hydrodeoxygenation. *Appl. Catal. B Environ.* **2019**, *241*, 81–88.

(25) Frank, B.; Friedel, K.; Girgsdies, F.; Huang, X.; Schlögl, R.; Trunschke, A. CNT-supported Mo_xC catalysts: Effect of loading and carburization parameters. *ChemCatChem* **2013**, *5* (8), 2296–2305.

(26) Cattelan, L.; Yuen, A. K. L.; Lui, M. Y.; Masters, A. F.; Selva, M.; Perosa, A.; Maschmeyer, T. Renewable aromatics from kraft lignin with molybdenum-based catalysts. *ChemCatChem* **2017**, *9* (14), 2717–2726.

(27) Baddour, F. G.; Nash, C. P.; Schaidle, J. A.; Ruddy, D. A. Synthesis of α-MoC_{1-x} nanoparticles with a surface-modified SBA-15 hard template: Determination of structure-function relationships in acetic acid deoxygenation. *Angew. Chem. Int. Ed.* **2016**, *55* (31), 9026–9029.

(28) Ren, P.; Zhao, Z. Unexpected coke-resistant stability in steam-CO_2 dual reforming of methane over the robust Mo_2C-Ni/ZrO_2 catalyst. *Catal. Commun.* **2019**, *119*, 71–75.

(29) Rocha, A. S.; Souza, L. A.; Oliveira, R. R.; Rocha, A. B.; Teixeira da Silva, V. Hydrodeoxygenation of acrylic acid using Mo_2C/Al_2O_3. *Appl. Catal. Gen.* **2017**, *531*, 69–78.

(30) Aegerter, P. A.; Quigley, W. W. C.; Simpson, G. J.; Ziegler, D. D.; Logan, J. W.; McCrea, K. R.; Glazier, S.; Bussell, M. E. Thiophene hydrodesulfurization over alumina-supported molybdenum carbide and nitride catalysts: Adsorption sites, catalytic activities, and nature of the active surface. *J. Catal.* **1996**, *164* (1), 109–121.

(31) Wu, W.; Wu, Z.; Liang, C.; Ying, P.; Feng, Z.; Li, C. An IR study on the surface passivation of Mo_2C/Al_2O_3 catalyst with O_2, H_2O and CO_2. *Phys. Chem. Chem. Phys.* **2004**, *6* (24), 5603–5608.

(32) Christofoletti, T.; Assaf, J. M.; Assaf, E. M. Methane steam reforming on supported and non-supported molybdenum carbides. *Chem. Eng. J.* **2005**, *106* (2), 97–103

(33) Mortensen, P. M.; de Carvalho, H. W. P.; Grunwaldt, J.-D.; Jensen, P. A.; Jensen, A. D. Activity and stability of Mo_2C/ZrO_2 as catalyst for hydrodeoxygenation of mixtures of phenol and 1-octanol. *J. Catal.* **2015**, *328*, 208–215.

(34) Boullosa-Eiras, S.; Lødeng, R.; Bergem, H.; Stöcker, M.; Hannevold, L.; Blekkan, E. A. Catalytic hydrodeoxygenation (HDO) of phenol over supported molybdenum carbide, nitride, phosphide and oxide catalysts. *Catal. Today* **2014**, *223*, 44–53.

(35) Oyama, S. T. Preparation and catalytic properties of transition metal carbides and nitrides. *Catal. Today* **1992**, *15* (2), 179–200.

(36) Hanif, A.; Xiao, T.; York, A. P. E.; Sloan, J.; Green, M. L. H. Study on the structure and formation mechanism of molybdenum carbides. *Chem. Mater.* **2002**, *14* (3), 1009–1015

(37) Xiao, T.; York, A. P.; Coleman, K. S.; Claridge, J. B.; Sloan, J.; Charnock, J.; Green, M. L. Effect of carburising agent on the structure of molybdenum carbides. *J. Mater. Chem.* **2001**, *11* (12), 3094–3098.

(38) Xiao, T.; York, A. P. E.; Williams, V. C.; Al-Megren, H.; Hanif, A.; Zhou, X.; Green, M. L. H. Preparation of molybdenum carbides using butane and their catalytic performance. *Chem. Mater.* **2000**, *12* (12), 3896–3905.

(39) Mo, T.; Xu, J.; Yang, Y.; Li, Y. Effect of carburization protocols on molybdenum carbide synthesis and study on its performance in CO hydrogenation. *Catal. Today* **2016**, *261*, 101–115.

(40) Chary, K. V. R.; Bhaskar, T.; Seela, K. K.; Sri Lakshmi, K.; Reddy, K. R. Characterization and reactivity of molybdenum oxide catalysts supported on anatase and rutile polymorphs of titania. *Appl. Catal. Gen.* **2001**, *208* (1–2), 291–305.

(41) Budroni, G.; Corma, A. Gold and gold–platinum as active and selective catalyst for biomass conversion: Synthesis of γ-butyrolactone and one-pot synthesis of pyrrolidone. *J. Catal.* **2008**, *257* (2), 403–408.

(42) Tapin, B.; Epron, F.; Especel, C.; Ly, B. K.; Pinel, C.; Besson, M. Study of monometallic Pd/TiO_2 catalysts for the hydrogenation of succinic acid in aqueous phase. *ACS Catal.* **2013**, *3* (10), 2327–2335.

(43) Shao, Z.; Li, C.; Di, X.; Xiao, Z.; Liang, C. Aqueous-phase hydrogenation of succinic acid to γ-butyrolactone and tetrahydrofuran over Pd/C, Re/C, and Pd–Re/C Catalysts. *Ind. Eng. Chem. Res.* **2014**, *53* (23), 9638–9645.

(44) Di, X.; Shao, Z.; Li, C.; Li, W.; Liang, C. Hydrogenation of succinic acid over supported rhenium catalysts prepared by the microwave-assisted thermolytic method. *Catal. Sci. Technol.* **2015**, *5* (4), 2441–2448.

(45) Ly, B. K.; Minh, D. P.; Pinel, C.; Besson, M.; Tapin, B.; Epron, F.; Especel, C. Effect of addition mode of Re in bimetallic Pd–Re/TiO_2 catalysts upon the selective aqueous-phase hydrogenation of succinic acid to 1,4-butanediol. *Top. Catal.* **2012**, *55* (7–10), 466–473.

(46) Ly, B. K.; Tapin, B.; Aouine, M.; Delichere, P.; Epron, F.; Pinel, C.; Especel, C.; Besson, M. Insights into the oxidation state and location of rhenium in Re-Pd/TiO_2 catalysts for aqueous-phase selective hydrogenation of succinic acid to 1,4-butanediol as a function of palladium and rhenium deposition methods. *ChemCatChem* **2015**, *7* (14), 2161–2178.

(47) Kitsiou, P.; Lagopati, N.; Tsilibary, E.-P.; Falaras, P.; Papazafiri, P.; Pavlatou, E. P.; Kotsopoulou, E. Effect of nanostructured TiO_2 crystal phase on photoinduced apoptosis of breast cancer epithelial cells. *Int. J. Nanomedicine* **2014**, *9*, 3219–3230.

(48) Ferrari, A. C.; Robertson, J. Raman spectroscopy of amorphous, nanostructured, diamond–like carbon, and nanodiamond. *Philos. Trans. R. Soc. Lond. A* **2004**, *362*, 2477–2512.

(49) Pimenta, M. A.; Dresselhaus, G.; Dresselhaus, M. S.; Cançado, L. G.; Jorio, A.; Saito, R. Studying disorder in graphite-based systems by raman spectroscopy. *Phys Chem Chem Phys* **2007**, *9* (11), 1276–1290.

(50) Li, H.; Hong, W.; Cui, Y.; Fan, S.; Zhu, L. Effect of Mo_2C content on the structure and photocatalytic property of Mo_2C/TiO_2 catalysts. *J. Alloys Compd.* **2013**, *569*, 45–51.

(51) Bouchy, C.; Hamid, S. B. D.-A.; Derouane, E. G. A new route to the metastable fcc molybdenum carbide α-MoC_{1-x}. *Chem Commun* **2000**, *2*, 125–126.

(52) Delporte, P.; Meunier, F.; Pham-Huu, C.; Vennegues, P.; Ledoux, M. J.; Guille, J. Physical characterization of molybdenum oxycarbide catalyst; TEM, XRD and XPS. *Catal. Today* **1995**, *23* (3), 251–267.

(53) Hanaor, D. A. H.; Sorrell, C. C. Review of the anatase to rutile phase transformation. *J. Mater. Sci.* **2011**, *46* (4), 855–874.

(54) Quincy, R. B.; Houalla, M.; Proctor, A.; Hercules, D. M. Distribution of molybdenum oxidation states in reduced molybdenum/titania catalysts: Correlation with benzene hydrogenation activity. *J. Phys. Chem.* **1990**, *94* (4), 1520–1526.

(55) Busca, G. *Heterogeneous catalytic materials: Solid state chemistry, surface chemistry and catalytic behaviour*; Elsevier, Amsterdam, 2014; pp. 162.

(56) Oshikawa, K.; Nagai, M.; Omi, S. Characterization of molybdenum carbides for methane reforming by TPR, XRD, and XPS. *J. Phys. Chem. B* **2001**, *105* (38), 9124–9131.

(57) Smirnov, A. A.; Geng, Zh.; Khromova, S. A.; Zavarukhin, S. G.; Bulavchenko, O. A.; Saraev, A. A.; Kaichev, V. V.; Ermakov, D. Yu.; Yakovlev, V. A. Nickel molybdenum carbides: Synthesis, characterization, and catalytic activity in hydrodeoxygenation of anisole and ethyl caprate. *J. Catal.* **2017**, *354*, 61–77.

(58) Perret, N.; Wang, X.; Delannoy, L.; Potvin, C.; Louis, C.; Keane, M. A. Enhanced selective nitroarene hydrogenation over Au supported on β-Mo_2C and β-Mo_2C/Al_2O_3. *J. Catal.* **2012**, *286*, 172–183.

(59) Mir, R. A.; Sharma, P.; Pandey, O. P. Thermal and structural studies of carbon coated Mo_2C synthesized via in-situ single step reduction-carburization. *Sci. Rep.* **2017**, *7* (1), 3518.

(60) Ostrovski, O.; Zhang, G. Reduction and carburization of metal oxides by methane-containing Gas. *AIChE J.* **2006**, *52* (1), 300–310.

(61) Vo, D.-V. N.; Adesina, A. A. Kinetics of the carbothermal synthesis of Mo carbide catalyst supported on various semiconductor oxides. *Fuel Process. Technol.* **2011**, *92* (6), 1249–1260.

(62) Shao, Z.; Li, C.; Di, X.; Xiao, Z.; Liang, C. Aqueous-phase hydrogenation of succinic acid to γ-butyrolactone and tetrahydrofuran over Pd/C, Re/C, and Pd–Re/C Catalysts. *Ind. Eng. Chem. Res.* **2014**, *53* (23), 9638–9645.

(63) Liu, X.; Wang, X.; Xu, G.; Liu, Q.; Mu, X.; Liu, H. Tuning the catalytic selectivity in biomass-derived succinic acid hydrogenation on FeO_x -Modified Pd Catalysts. *J. Mater. Chem. A* **2015**, *3* (46), 23560–23569.

(64) You, C.; Zhang, C.; Chen, L.; Qi, Z. Highly dispersed palladium nanoclusters incorporated in amino-functionalized silica spheres for the selective hydrogenation of succinic acid to γ-butyrolactone: Amino-functionalized Pd catalysts for succinic acid hydrogenation. *Appl. Organomet. Chem.* **2015**, *29* (10), 653–660.

(65) Hong, U. G.; Hwang, S.; Seo, J. G.; Lee, J.; Song, I. K. Hydrogenation of succinic acid to γ-butyrolactone (GBL) over palladium catalyst supported on alumina xerogel: Effect of acid density of the catalyst. *J. Ind. Eng. Chem.* **2011**, *17* (2), 316–320.

(66) Rocha A. S.; Souza L. A.; Oliveira R. R.; Rocha A. B.; Teixeira da Silva. Hydrodeoxygenation of acrylic acid using Mo_2C/Al_2O_3. V. *Appl. Catal. Gen.* **2017,** *531*, 69–78.

(67) Herrmann, U; Emig, G. Liquid phase hydrogenation of maleic anhydride and intermediates on copper-based and noble metal catalysts. *Ind. Eng. Chem. Res.* **1997**, *36*, 2885–2896.

(68) Vardon, D. R.; Settle, A. E.; Vorotnikov, V.; Menart, M. J.; Eaton, T. R.; Unocic, K. A.; Steirer, K. X.; Wood K. N.; Cleveland N. S.; Moyer K. E.; Michener W. E.; Beckham G. T. Ru-Sn/AC for the aqueous-phase reduction of succinic acid to 1,4‑butanediol under continuous process conditions. *ACS Catal.* **2017**, *7*, 6207–6219.

(69) Ftouni, J.; Muñoz-Murillo, A.; Goryachev, A.; Hofmann, J. P.; Hensen, E. J. M.; Lu, L.; Kiely, C. J.; Bruijnincx, P. C. A.; Weckhuysen, B. M. ZrO_2 is preferred over TiO_2 as support for the Ru-catalyzed hydrogenation of levulinic acid to γ-valerolactone. *ACS Catal.* **2016**, *6* (8), 5462–5472.

(70) Schaidle, J. A.; Blackburn, J.; Farberow, C. A.; Nash, C.; Steirer, K. X.; Clark, J.; Robichaud, D. J.; Ruddy D. A. Experimental and computational investigation of acetic acid D=deoxygenation over oxophilic molybdenum carbide: Surface chemistry and active site identity. *ACS Catal.* **2016**, *6*, 1181–1197.

(71) Wang, T.; Tian, X.; Yang, Y.; Li, Y.-W.; Wang, J.; Beller M.; Jiao, H. Coverage dependent adsorption and co-adsorption of CO and H_2 on the CdI_2-antitype metallic Mo_2C(001) surface. *Phys. Chem. Chem. Phys.* **2015,** *17*, 1907–1917.

(72) Elvers, B.; Hawkins, S.; Russey, W. E. *Ullmann's Encyclopedia of Industrial Chemistry*; Wiley-VCH, Weinheim, 2003, Vol. 40; pp. 15.

(73) Butyric Acid Market. In *Market Research Report*; CH 3662, 2015.

Table of Contents graphic: